Published in final edited form as:
Cancer Res. 2009 July 1; 69(13): 5601–5609. doi:10.1158/0008-5472.CAN-08-3860.

Oncosome formation in prostate cancer: Association with a region of frequent chromosomal deletion in metastatic disease

Dolores Di Vizio[1,2], **Jayoung Kim**[1,2], **Martin H. Hager**[1], **Matteo Morello**[1], **Wei Yang**[1], **Christopher J. Lafargue**[5], **Lawrence True**[4], **Mark A. Rubin**[5], **Rosalyn M. Adam**[1,2], **Rameen Beroukhim**[6,7,8], **Francesca Demichelis**[5,9], and **Michael R. Freeman**[1,2,3]

[1] The Urological Diseases Research Center, Children's Hospital Boston, Boston, MA

[2] Departments of Surgery, Harvard Medical School, Boston, MA

[3] Biological Chemistry and Molecular Pharmacology, Harvard Medical School, Boston, MA

[4] Department of Pathology, University of Washington Medical Center, Seattle, WA

[5] Department of Pathology and Laboratory Medicine, Weill Cornell Medical College, New York, NY

[6] Broad Institute of MIT and Harvard, Cambridge, MA

[7] Department of Medical Oncology, Dana-Farber Cancer Institute, Harvard Medical School, Boston, MA

[8] Department of Medicine, Brigham and Women's Hospital, Harvard Medical School, Boston, MA

[9] Institute for Computational Biomedicine, Weill Cornell Medical College, New York, NY

Abstract

Oncosomes have recently been described as membrane-derived microvesicles secreted by cancer cells, which transfer oncogenic signals and protein complexes across cell boundaries. Here we demonstrate the rapid formation and secretion of oncosomes from DU145 and LNCaP human prostate cancer cells. Oncosome formation was stimulated by EGFR activation and also by over-expression of membrane-targeted Akt1. Microvesicles shed from prostate cancer cells contained numerous signal transduction proteins and were capable of activating rapid phospho-tyrosine and Akt pathway signaling, and stimulating proliferation and migration, in recipient tumor cells. They also induced a stromal reaction in recipient normal cells. Knockdown of the actin nucleating protein Diaphanous Related Formin 3 (DRF3/Dia2) by RNA interference enhanced rates of oncosome formation, indicating that these structures resemble, and may be identical to, non-apoptotic membrane blebs, a feature of the amoeboid form of cell motility. Analysis of primary and metastatic human prostate tumors using 100K SNP arrays revealed a significantly higher frequency of deletion of the locus encoding DRF3 (DIAPH3) in metastatic tumors (p=0.001) in comparison with organ-confined tumors. Fluorescence in situ hybridization (FISH) confirmed increased chromosomal loss of DIAPH3 in metastatic tumors in a different cohort of patients (p=0.006). These data suggest that microvesicles shed from prostate cancer cells can alter the tumor microenvironment in a manner that may promote disease progression. They also show that DRF3 is a physiologically relevant protein that appears to regulate this process.

Correspondence: Michael R. Freeman, PhD, Enders Research Laboratories, Rm 1161, Children's Hospital Boston, 300 Longwood Ave. Boston, MA 02115, Tel: 617-919-2644, Fax: 617-730-0238, michael.freeman@childrens.harvard.edu.

Keywords

Metastasis; tumor microenvironment; actin; Diaphanous; Caveolin-1

Introduction

Prostate cancer (PCa) is a major cause of cancer-related death in Western countries. While the majority of cancers are unlikely to progress to end-stage disease, castration-resistant PCa is still a major clinical challenge. The development of effective therapies for advanced PCa requires an understanding of the processes that promote the metastatic state. Cancer cells colonize distant sites using several strategies, including production of proteases that degrade extracellular matrix (1), and extension of lamellipodia, filopodia, and other dynamic cell processes that mediate migration (2). Formation of lamellipodia, which generate force at the front end of a migrating cell, requires actin filament assembly and the coordinated activity of multiple protein complexes that regulate assembly and disassembly of the cytoskeleton (3).

A less studied mode of cell motility, termed “amoeboid” movement, occurs as a result of non-apoptotic blebbing (4,5). Plasma membrane blebs arise from actomyosin contractions near the cortical cytoskeleton, which create the opportunity for rapidly forming membrane protrusions to arise from hydrostatic pressure. Actin filament assembly is not required for the formation of non-apoptotic blebs, but force generated by actin filaments is required for bleb retraction. Bleb-associated movement is mediated by Rho-GTPase/ROCK signaling (6) and generates propulsive motion through a 3-dimensional matrix in a manner that requires limited or no proteolysis (7). The mechanisms that control the amoeboid phenotype in tumor cells are poorly understood, as is the role of this process in malignant progression.

Oncosomes are recently discovered membranous microvesicles that have been implicated in rapid intercellular transfer of oncogenic information from glioblastoma to indolent glioma cells (8). Although this process resembles paracrine signaling, it involves inter-cellular transfer of a membrane-bound micro-organelle rather than a soluble protein such as a growth factor or cytokine. In the present study we demonstrate that PCa cells shed membrane-bound vesicles in response to signal transducers. These structures are fairly large (0.5 to ~5μm), originate from non-apoptotic blebs in response to signaling cues, and have biological activity in their free-floating state. We also identify the formin homology (FH) protein, DRF3/Dia2, as a protein that appears to functionally inhibit oncosome formation. We also provide the first evidence that chromosomal loss at the DRF3 locus (DIAPH3) is associated with metastatic PCa. Our results suggest the novel possibility that oncosomes may play a role in progression to metastatic disease through the controlled export of oncogenic protein complexes.

Materials and Methods

Reagents

Antibodies were from Biosource, Camarillo, CA; Cell Signaling, Beverly, MA; BD Transduction, Franklin Lakes, NJ; Santa Cruz Biotechnologies, Santa Cruz, CA; Sigma, St. Louis, MO; Covance, Inc. NJ; and Upstate, Lake Placid, NY. ZD1839 (gefitinib) was from AstraZeneca, Macclesfield, UK. FuGENE6 was from Roche (Indianapolis, IN). Other reagents were from Sigma. Anti-DRF3 mAb was a gift from Dr. H. Higgs (Dartmouth).

Cell culture and transfections

DU145, LNCaP and WPMY-1 cell lines were from the ATCC. hTERT-immortalized normal prostate epithelial cells (iPrEC), generously provided by Dr. W. Hahn (Dana-Farber Cancer

Institute) were kept in PrEGM medium. Stable transfectant cell populations (MyrAkt1, LacZ, HB-EGF and Vo) were described (9,10). Transient transfection (Cav-1-GFP (11) or pMEM-YFP (12)) were performed using FuGENE6. These constructs were generously provided by Dr. M. Lisanti (Thomas Jefferson University) and Dr. D. Clapham (Harvard Medical School), respectively.

Immunofluorescence microscopy

Cell membranes were labeled with FITC-conjugated cholera toxin B (CTxB) subunit (Sigma, St. Louis, MO) or Alexa 594–conjugated CTxB (Molecular Probes, Carlsbad, CA) and analyzed as previously described (13).

Isolation of oncosomes and oncosome transfer assays

Shed microvesicles were collected from conditioned medium and purified essentially as described (8). Briefly, medium was subjected to two successive, rapid centrifugations at 300*g* and 12,000*g* to eliminate cells and debris. Microvesicles were then pelleted by ultracentrifugation for 2 h at 100,000*g*. Recovered material was resuspended in ice-cold PBS and quantified by measuring protein content. Recipient cells were serum-starved for 12 h and were subsequently treated with 20μg of ultracentrifuged material.

Silencing of DRF3 expression

DU145 cells were transfected with ON-TARGETplus SMARTpool siRNA duplexes for the target sequence NM_030932, or with control non-targeting siRNA (Dharmacon Inc., Lafayette, CO) using DharmaFECT1 reagent, for 72 h. RT-PCR and WB were used to validate specific silencing of DRF3 expression. *DIAPH3* gene-specific primer pair (5′-TATATAGGTACCGCCAC CATGGAACGGCACCAGCCGCGGC-3′/5′-AAGTTGGATATCCAGGCCATC-3′) was used for the RT-PCR, and PCR products analyzed by agarose gel electrophoresis.

Mass spectrometry and label-free quantification

SDS-PAGE gel slices were subjected to in-gel digestion as described (14). Tryptic peptides were separated at circa 400nl/min with 60 min linear gradients from 5 to 31% acetonitrile in 0.4% formic acid and analyzed using an LTQ ProteomeX ion trap mass spectrometer (Thermo Finnigan, San Jose, CA). Database searches were performed as described (13) except that mass tolerance was set at ±1.5 Da for MS/MS spectra. Proteins were identified with at least 2 unique peptides, with each peptide having an ion score no less than 40 ($p<0.05$). Relative protein abundance was determined using label-free spectral counting (15).

Pathway enrichment and network analysis

The integrated software suite MetaCore (GeneGo, St. Joseph, MI) was used to map proteins into biological networks of human protein-protein, protein-DNA and protein-compound interactions, metabolic and signaling pathways (http://www.genego.com). For network analysis, two algorithms were used: 1) the direct interaction algorithm to map direct protein-protein interaction; 2) the shortest path algorithm to map the shortest interaction pathway.

Cell proliferation and migration assays

Cell proliferation was determined by viability assay (10). Cell migration was assessed using 1) in vitro wound healing assay and 2) cell migration chambers (Chemicon International Inc., Temecula, CA).

SNP arrays

Human specimen collection and preparation have been described (16). Genomic DNA was hybridized to 100K SNP arrays (Affymetrix, Santa Clara, CA) according to the manufacturer's instructions. Arrays were scanned with a GeneChip Scanner 3000, and genotyping was performed using Affymetrix Genotyping Tools Version 2.0. Probe-level signal intensities were normalized to a baseline array using invariant set normalization (17). SNP-level signal intensities were obtained using a model-based (PM/MM) method (17). Tumor data were normalized against data from normal tissue samples selected for similar baseline noise characteristics (18). Noise was further reduced using the segmentation algorithm Gain and Loss Analysis of DNA (19). Histogram analysis (18) was used to confirm that all tumors were sufficiently enriched to observe copy-number changes. Deletion at the DIAPH3 locus was identified as segmented log2 ratio < -0.1, a value reached in only 0.5% of SNPs in data from normal tissue.

Dual Color FISH

DIAPH3 gene alteration was assessed by FISH on TMA sections with tissue samples from radical prostatectomy and a prostate cancer progression TMA (20). For the DIAPH3 target probe, spanning the DIAPH3 locus (chr13q21.2), the Biotin-14-dCTP labeled BAC clones RP11-643G22 and RP11-638B12 (eventually conjugated to produce a red signal) were applied. For the reference probe, used to evaluate tumor cell ploidy on a stable area of chromosome 21, the Digoxigenin-11-dUTP labeled BAC clone RP11-451M12 (eventually conjugated to produce a green signal) was applied. The BAC clones were from the BACPAC Resourch Center, Children's Hospital Oakland Research Institute (CHORI) (Oakland, CA). Correct chromosomal probe localization was confirmed on normal lymphocytes metaphase preparations. Tissue hybridization, washing, and color detection were performed as described (21). The samples were analyzed under a 60x oil immersion objective using an Olympus BX-511 fluorescence microscope, a CCD camera and the CytoVision FISH software (Applied Imaging, San Jose, CA). Semiquantitative evaluation of the tests was performed by D.D.V. and C.J.L. on at least 50 nuclei.

Real time RT-PCR

Total RNA was isolated from WPMY-1 using TRIzol reagent, further purified using RNeasy columns and reverse- transcribed using iScript reagent (BioRad Laboratories, Hercules, CA), according to the manufacturer's instructions. cDNAs were amplified with gene-specific primers for vimentin, or GAPDH using SYBR® Green qPCR Master Mix. Human PRKAR1A was used as an irrelevant gene. The relative abundance of a given transcript in control and treated cells was estimated by comparing the cycle threshold (Ct) values for each sample following normalization to GAPDH.

Results

Inducible formation of non-apoptotic blebs in prostate cancer cells

In experiments where DU145 human PCa cells were stimulated with EGF, we noted extensive membrane blebbing (Fig. 1), which occurred immediately (~5 min) following growth factor treatment and persisted for 24 h (Supplemental Fig. S1). Newly formed blebs were predominantly 0.5–5 μm in diameter and could be labeled with the ganglioside probe cholera toxin B subunit (CTxB; Fig. 1A), a membrane-directed yellow fluorescent protein (pMEM-YFP) (12) (Fig. 1B) or the plasma membrane glycoprotein probe wheat germ agglutinin (not shown). Sporadic bleb formation was also observed in vehicle-treated cells. Blebbing did not coincide with increased rates of cell death (Fig. 1D), indicating that these structures are non-apoptotic membrane blebs described in other cell types (22–26) but not to our knowledge in

prostatic cells. Similar rapid blebbing was evoked from the PC-3 human PCa cell line in response to EGF (Fig. 1A).

Live confocal imaging of DU145 cells expressing pMEM-YFP and treated with EGF showed blebs emerging rapidly as protrusions, which were sometimes retracted (Fig. 1B and Movie 1). Blebs were also completely extruded from the cell body and released into the medium (Fig. 1A, 1C and Movie 2). Isolation of shed vesicles (SV) by collection of media and ultracentrifugation indicated that they contained the membrane protein caveolin-1 (Cav-1; Fig. 1D), a PCa serum biomarker and an indicator of advanced disease (27). Consistent with this observation, blebs could also be decorated with Cav-1-GFP (Fig. 1D). An in vitro wound healing assay showed that rates of bleb formation correlated with increased cell migration (Fig. 2A). The increase in rates of blebbing in response to EGF was completely suppressed by the EGFR inhibitor gefitinib (Fig. 2Bi).

We observed spontaneous blebbing in LNCaP PCa cells, however basal rates of bleb formation were lower in LNCaP than in DU145, a more aggressive cell line. To determine whether blebbing would increase in response to activation of oncogenic signaling, we assessed the extent of bleb formation in LNCaP cells stably expressing the potent membrane-directed oncoprotein MyrAkt1 (9), the membrane-associated precursor form of the EGFR ligand HB-EGF (proHB-EGF), or a soluble form of HB-EGF (sHB-EGF) that is released constitutively into the medium (10). Blebbing was significantly increased in LNCaP cells expressing either proHB-EGF or sHB-EGF in the absence of exogenous EGF (Fig. 2C). Addition of EGF further increased blebbing in MyrAkt1- and proHB-EGF-expressing cells (Fig. 2C). Consistent with their sustained export of high levels of sHB-EGF, EGF did not have a further stimulatory effect on LNCaP/sHB-EGF cells. Bleb formation in normal prostate epithelial and stromal cells was modest and unresponsive to EGF (Fig. 2Bii), however in this case blebbing was not a reflection of EGFR level or sensitivity to ligand (Supplemental Fig. S1B).

Bleb secretions contain numerous signal transduction proteins

Because secreted vesicles (SV) contained Cav-1, we hypothesized that they might contain other signaling proteins as cargo. SV from LNCaP/MyrAkt1 and LNCaP cells transfected with an irrelevant gene (LacZ) were isolated by collection of medium, followed by ultracentrifugation. SV contained the membrane-associated proteins Akt and Src (Fig. 2D), however we did not detect the largely nuclear androgen receptor (AR) and the predominantly cytosolic enzyme fatty acid synthase (FASN), both of which are expressed at high levels in LNCaP cells. We detected HA-tagged MyrAkt1 in SV from LNCaP/MyrAkt1 cells (Fig. 2D), however LNCaP/LacZ cells also produced SV that contained endogenous Akt1 (Supplemental Fig. S2A).

To identify protein cargo in SV in an unbiased manner, LNCaP/LacZ and LNCaP/MyrAkt1 SV protein was fractionated by SDS-PAGE. Two prominent zones containing the most abundant proteins ran at ~80 and ~30 kDa (Supplemental Fig. S2B). These zones were excised and analyzed by tandem mass spectrometry (LC-MS/MS). Each protein was identified from at least two unique peptides with an ion score of no less than 40 ($p<0.01$). SV proteins were sorted according to their MOWSE scores and semi-quantified using spectral counting (15). Numerous signaling proteins involved in cell metabolism, mRNA processing and cell growth and motility were identified (Fig. 3A and Supplemental Table S1). The majority of SV proteins were present in both sublines, although as shown, there were some quantitative differences (only proteins with less than 15 spectral counts in at least one sample are shown). This result suggests the possibility of changes in SV protein composition with alterations in signal transduction (e.g., upregulation Akt signaling in LNCaP/MyrAkt1 cells). Multiple proteins of potential relevance to cancer progression were found, including: (1) the cancer-cell-specific isoform of pyruvate kinase M2 (PKM2), a phosphotyrosine-binding protein that promotes increased cell growth and tumor development (28); (2) programmed cell death 6 interacting

protein (PDCD6IP), also known as Alix, recently shown to inhibit apoptosis (29); (3) poly(A)-binding protein 1 (PABPC1), which associates with paxillin and promotes cell migration; and (4) hnRNP-K, a multifunctional regulator of transcription and translation induced by extracellular growth promoting signals that enhance cancer cell proliferation (30).

Mass spectrometry data were analyzed using the MetaCore data mining tool (http://www.genego.com) in order to determine whether bleb/SV cargo could be organized into coherent networks and linked to one or more biological processes. Three statistically significant associations with GeneGo ontology pathway or biological process models, all related to mRNA translation, were identified using SV proteins from LNCaP/LacZ cells (Table 1). Interestingly, a much greater number of significant associations was detected using SV cargo from LNCaP/MyrAk1 cells (9 such associations with LNCaP/Akt1 cells vs. 3 seen with LNCaP/LacZ cells), including links to cytoskeletal rearrangement, cell cycle progression, inflammation, DNA damage, cell adhesion and mRNA translation. These data suggest the possibility that the vesicles originating from plasma membrane blebs might be able to relay signals across cell boundaries in a manner similar to recently described glioblastoma-derived oncosomes (8).

Horizontal signaling

Because analysis of LNCaP SV cargo suggested that the bleb-derived material might possess bioactivities described for oncosomes, we asked whether LNCaP/MyrAkt1 SV are capable of altering signal transduction in recipient cells in a horizontal fashion. SV were isolated from LNCaP/MyrAkt1 cells and recovered material was quantified by determining protein content. Recipient LacZ cells exposed to SV from LNCaP/MyrAkt1 cells showed a time-dependent activation of the Akt pathway (Fig. 3B), as assessed using a consensus Akt phosphorylated substrate antibody (31). Consistent with this, levels of active Akt1 (p-S473) and its phosphorylated targets GSK3α/β (p-S21/9) and FoxO1 (p-S256) increased in a time dependent manner. In these experiments, HA-tagged MyrAkt1 was transferred to recipient cells (Fig. 3B, arrow). This finding demonstrates that vesicles shed by LNCaP/MyrAkt1 cells possess activities associated with oncosomes. They also show that an oncoprotein (MyrAkt1) can be transferred across cell boundaries with SV as a vehicle. Consistent with these data, LNCaP/MyrAkt1 SV also evoked robust p-Tyr signaling and EGFR pathway activation in recipient cells (Fig. 3C). SV material also elicited increased levels of vimentin mRNA in WPMY-1 prostate stromal cells (Fig. 3D), suggesting that the vesicles are capable of evoking a stromal reaction (32).

The actin nucleating protein DRF3/Dia2 inhibits bleb formation

Non-apoptotic membrane blebbing arises from membrane deformations resulting from actomyosin contraction (4) and has been linked to amoeboid cell motility and matrix invasion (23). These findings imply that actin remodeling may affect oncosome formation. To test this idea, we focused on DRF3 (Diaphanous Related Formin 3), the human homolog of the mouse actin nucleating protein Drf3/mDia2 (33). DRF3 is encoded on chromosome 13q, which contains a region of genomic instability in PCa (34). An inhibitor of Drf3 was recently reported to induce non-apoptotic blebbing (35), suggesting the possibility that DRF3 may oppose blebbing.

DRF3 knockdown by RNA interference (RNAi), using a pool of four siRNA oligos targeted to DRF3, dramatically increased bleb formation in the presence of EGF (Fig. 4A–C), a result that implicates cytoskeletal dynamics in the blebbing process. To determine whether SV derived from cells in which DRF3 had been knocked-down would affect cell behavior in recipient cells, we performed proliferation and migration assays using DU145 cells exposed to SV derived from DU145 cells in which DRF3 expression was reduced by RNAi. Cell

proliferation and migration were increased in recipient cells exposed to SV isolated from DU145 cells treated with DRF3 siRNA, at a level quantitatively comparable to that elicited in donor cells by activation of EGFR alone (Fig. 4D).

Frequent chromosomal deletions at the DIAPH3 locus in metastatic prostate cancer

The above findings suggest that DRF3 is capable of inhibiting the blebbing/amoeboid phenotype. To determine the potential relevance of these observations to human PCa, we evaluated the human DRF3 locus (DIAPH3) for chromosomal alterations using 100K SNP arrays, profiling 12 primary PCa tumors and 27 metastatic tumors. A total of 19 (49%) of these tumors exhibited deletions at the DIAPH3 locus (Fig. 5A), much higher than the overall 20% rate of deletion across the genome. Although all of these tumors, including the primaries, were sufficiently enriched to observe copy-number changes elsewhere in the genome, at the DIAPH3 locus deletions were observed more frequently among metastases (18 out of 27 (67%)) than primaries (1 out of 12 (8.3%)) (2-sided Fisher's exact test, $p = 0.001$). In a different cohort of patient samples, fluorescence in situ hybridization (FISH), an alternative method, was used to assess the DIAPH3 locus for chromosomal alterations. FISH results indicated chromosomal loss of DIAPH3 in 7 out of 35 (20%) primaries, and 9 out of 14 (64%) metastases (Fig. 5B), confirming a significantly higher frequency of deletions in aggressive disease in comparison with primary tumors (2-sided Fisher's exact test, $p = 0.006$). DIAPH3 deletion was not detected in benign tissues.

Discussion

In this study we describe the production of non-apoptotic membrane blebs in human PCa cells in response to activation of oncogenic signaling (EGFR and Akt activation). Formation of these dynamic structures correlates with cell migration and, when shed from tumor cells, they elicit biological responses in recipient cells in a manner that resembles--but is mechanistically distinct from--paracrine signaling. We conclude that the microvesicles we have studied here are functionally equivalent to the bioactive oncosomes recently described as products of aggressive glioblastoma cells (8). We also identify the actin nucleating protein DRF3 as an endogenous inhibitor of oncosome formation. Analysis of primary and metastatic prostate tumors using high density SNP arrays and FISH resulted in a highly significant association between chromosomal loss at the DRF3 (DIAPH3) locus and metastatic disease. To our knowledge, this is the first study that describes oncosome formation by PCa cells, the first to link formation of SV with non-apoptotic blebbing, and the first to provide evidence for involvement of the formin DRF3 in metastases in any tumor system. Oncosome activity was demonstrated in two unrelated PCa cell line backgrounds, LNCaP and DU145, and similar membrane blebbing was evoked in PC-3 cells in response to EGF, suggesting that this is a general phenomenon. The precise relationship between the surprisingly large (0.5–5μm) SV we have observed here by fluorescence microscopy, using several membrane probes, and the smaller (<0.1–1 μm) secreted vesicles reported by other groups (36,37) remains to be determined.

The results of unbiased mass spectrometry studies, analysis of known proteins, and bioinformatics evaluation of SV cargo proteins are consistent with the finding that oncosome formation can result in transfer of membrane-associated protein complexes within the tumor microenvironment. Oncosomes might also be vectors of certain cancer progression markers that are detectable in the circulation. One such marker, Cav-1, identified in our study as oncosome cargo, is a circulating biomarker of metastatic PCa (13,27,38). Our data suggest that oncosome secretion is a mechanism whereby the integral membrane protein Cav-1 obtains access to the extracellular space, where it then becomes available to act at distant sites. Another SV cargo protein identified by mass spectrometry is hnRNP-K, which we recently showed to

be a novel Akt binding protein and regulator of AR translation (39). mRNA translation was repeatedly identified in the present study using the MetaCore software tool as a biological process that was significantly associated with bleb cargo proteins.

Our data indicate that the actin nucleator DRF3 is capable of inhibiting oncosome formation, since DRF3 knockdown by RNAi increased blebbing in DU145 cells, particularly in the presence of EGF. DRF3 is expressed by LNCaP, DU145 and PC-3 human prostate cell lines (data not shown). Formin homology (FH) proteins mediate cytoskeletal dynamics (9,35) and, as a group, have been implicated in a wide range of cellular functions, including motility and vesicular trafficking (40,41). The formin FHOD1, which exhibits 45% sequence homology to DRF3, was recently implicated in Src-dependent plasma membrane blebbing (42). Human DRF3 is not well studied, although analyses of the mouse homolog Drf3, and the close mouse paralog, Drf1/mDia1, indicate that DRF3 likely mediates actin filament nucleation and elongation (43) and microtubule stability (44). A DRF3 interactor, the Diaphanous interacting protein DIP, was recently shown to promote plasma membrane blebbing by acting as a Dia inhibitor (35). Non-apoptotic membrane blebs can either dissociate from the cell or be retracted in an actin-dependent manner (4). Blebbing has been linked to the amoeboid form of cell movement (45) and our data indicate that DRF3 likely plays a role within a critical signaling node that controls the amoeboid phenotype. The finding that DRF3 silencing in SV donor cells resulted in increased cell proliferation and migration in SV recipient cells provides an important new link between: (1) blebbing and the amoeboid phenotype and (2) the production of vesicles that can propagate signals horizontally in the tumor microenvironment. These experimental data are consistent with our analysis of human prostate tumors, indicating that chromosomal loss at the DRF3 coding region is associated with metastatic disease. Loss of function at the DIAPH3 locus from somatic mutation may lead to alterations in the propensity toward invasion or metastasis. We are currently testing this hypothesis experimentally.

Our experiments suggest that oncosome transfer between tumor cells, or between tumor and stroma, could play a role in propagation of aggressive behavior within the tumor microenvironment. As pointed out by Al-Nedawi et al. (8), oncosome exchange is markedly different from paracrine effects induced by soluble ligands. However, this process could result in amplification of paracrine pathways through intercellular sharing of membrane-associated signaling complexes. Although our study focuses on PCa, a similar microvesicular transfer mechanism may operate in other tumor systems.

Supplementary Material

Refer to Web version on PubMed Central for supplementary material.

Acknowledgments

This study was supported by NIDDK R3747556, P50 DK65298, NCI R01 CA112303 and DAMD17-03-2-0033 (to M.R.F), NCI K99 CA131472 (to D.D.V), DOD PCRP W81XWH-07-1-0148 (to M.H.H.), W81XWH-08-1-0139 (to W.Y.), the AUA Foundation/GlaxoSmithKline (to M.H.H.), the Pacific Northwest Prostate Cancer SPORE CA97186 and NCI P01CA085859 (to L.T.). J.K. is a Fishbein/ICA Scholar and a New York Academy of Medicine Edwin Beer Scholar. The authors thank Dr. H. Steen for assistance with mass spectrometry and Mr. Paul Guthrie for technical assistance.

References

1. Cao J, Chiarelli C, Richman O, Zarrabi K, Kozarekar P, Zucker S. Membrane type 1 matrix metalloproteinase induces epithelial-to-mesenchymal transition in prostate cancer. J Biol Chem 2008;283:6232–40. [PubMed: 18174174]
2. Wang HR, Zhang Y, Ozdamar B, et al. Regulation of cell polarity and protrusion formation by targeting RhoA for degradation. Science 2003;302:1775–9. [PubMed: 14657501]

3. Katoh H, Hiramoto K, Negishi M. Activation of Rac1 by RhoG regulates cell migration. J Cell Sci 2006;119:56–65. [PubMed: 16339170]
4. Paluch E, Sykes C, Prost J, Bornens M. Dynamic modes of the cortical actomyosin gel during cell locomotion and division. Trends Cell Biol 2006;16:5–10. [PubMed: 16325405]
5. Gadea G, Sanz-Moreno V, Self A, Godi A, Marshall CJ. DOCK10-mediated Cdc42 activation is necessary for amoeboid invasion of melanoma cells. Curr Biol 2008;18:1456–65. [PubMed: 18835169]
6. El-Sibai M, Pertz O, Pang H, et al. RhoA/ROCK-mediated switching between Cdc42- and Rac1-dependent protrusion in MTLn3 carcinoma cells. Exp Cell Res 2008;314:1540–52. [PubMed: 18316075]
7. Sahai E, Marshall CJ. Differing modes of tumour cell invasion have distinct requirements for Rho/ROCK signalling and extracellular proteolysis. Nat Cell Biol 2003;5:711–9. [PubMed: 12844144]
8. Al-Nedawi K, Meehan B, Micallef J, et al. Intercellular transfer of the oncogenic receptor EGFRvIII by microvesicles derived from tumour cells. Nat Cell Biol 2008;10:619–24. [PubMed: 18425114]
9. Adam RM, Mukhopadhyay NK, Kim J, et al. Cholesterol sensitivity of endogenous and myristoylated Akt. Cancer Res 2007;67:6238–46. [PubMed: 17616681]
10. Adam RM, Kim J, Lin J, et al. Heparin-binding epidermal growth factor-like growth factor stimulates androgen-independent prostate tumor growth and antagonizes androgen receptor function. Endocrinology 2002;143:4599–608. [PubMed: 12446587]
11. Volonte D, Galbiati F, Lisanti MP. Visualization of caveolin-1, a caveolar marker protein, in living cells using green fluorescent protein (GFP) chimeras. The subcellular distribution of caveolin-1 is modulated by cell-cell contact. FEBS Lett 1999;445:431–9. [PubMed: 10094502]
12. Oancea E, Wolfe JT, Clapham DE. Functional TRPM7 channels accumulate at the plasma membrane in response to fluid flow. Circ Res 2006;98:245–53. [PubMed: 16357306]
13. Adam RM, Yang W, Di Vizio D, Mukhopadhyay NK, Steen H. Rapid preparation of nuclei-depleted detergent-resistant membrane fractions suitable for proteomics analysis. BMC Cell Biol 2008;9:30. [PubMed: 18534013]
14. Yang W, Liu P, Liu Y, Wang Q, Tong Y, Ji J. Proteomic analysis of rat pheochromocytoma PC12 cells. Proteomics 2006;6:2982–90. [PubMed: 16622837]
15. Liu H, Sadygov RG, Yates JR 3rd. A model for random sampling and estimation of relative protein abundance in shotgun proteomics. Anal Chem 2004;76:4193–201. [PubMed: 15253663]
16. Hofer MD, Kuefer R, Huang W, et al. Prognostic factors in lymph node-positive prostate cancer. Urology 2006;67:1016–21. [PubMed: 16698361]
17. Li C, Wong WH. Model-based analysis of oligonucleotide arrays: expression index computation and outlier detection. Proc Natl Acad Sci U S A 2001;98:31–6. [PubMed: 11134512]
18. Beroukhim R, Getz G, Nghiemphu L, et al. Assessing the significance of chromosomal aberrations in cancer: methodology and application to glioma. Proc Natl Acad Sci U S A 2007;104:20007–12. [PubMed: 18077431]
19. Hupe P, Stransky N, Thiery JP, Radvanyi F, Barillot E. Analysis of array CGH data: from signal ratio to gain and loss of DNA regions. Bioinformatics 2004;20:3413–22. [PubMed: 15381628]
20. Di Vizio D, Adam RM, Kim J, et al. Caveolin-1 interacts with a lipid raft-associated population of fatty acid synthase. Cell Cycle 2008;7:2257–67. [PubMed: 18635971]
21. Perner S, Mosquera JM, Demichelis F, et al. TMPRSS2-ERG fusion prostate cancer: an early molecular event associated with invasion. Am J Surg Pathol 2007;31:882–8. [PubMed: 17527075]
22. Fackler OT, Grosse R. Cell motility through plasma membrane blebbing. J Cell Biol 2008;181:879–84. [PubMed: 18541702]
23. Gadea G, de Toledo M, Anguille C, Roux P. Loss of p53 promotes RhoA-ROCK-dependent cell migration and invasion in 3D matrices. J Cell Biol 2007;178:23–30. [PubMed: 17606864]
24. Voura EB, Sandig M, Siu CH. Cell-cell interactions during transendothelial migration of tumor cells. Microsc Res Tech 1998;43:265–75. [PubMed: 9840805]
25. Charras GT, Hu CK, Coughlin M, Mitchison TJ. Reassembly of contractile actin cortex in cell blebs. J Cell Biol 2006;175:477–90. [PubMed: 17088428]

26. Tournaviti S, Hannemann S, Terjung S, et al. SH4-domain-induced plasma membrane dynamization promotes bleb-associated cell motility. J Cell Sci 2007;120:3820–9. [PubMed: 17959630]
27. Tahir SA, Yang G, Ebara S, et al. Secreted caveolin-1 stimulates cell survival/clonal growth and contributes to metastasis in androgen-insensitive prostate cancer. Cancer Res 2001;61:3882–5. [PubMed: 11358800]
28. Christofk HR, Vander Heiden MG, Harris MH, et al. The M2 splice isoform of pyruvate kinase is important for cancer metabolism and tumour growth. Nature 2008;452:230–3. [PubMed: 18337823]
29. Chatellard-Causse C, Blot B, Cristina N, Torch S, Missotten M, Sadoul R. Alix (ALG-2-interacting protein X), a protein involved in apoptosis, binds to endophilins and induces cytoplasmic vacuolization. J Biol Chem 2002;277:29108–15. [PubMed: 12034747]
30. Mandal M, Vadlamudi R, Nguyen D, et al. Growth factors regulate heterogeneous nuclear ribonucleoprotein K expression and function. J Biol Chem 2001;276:9699–704. [PubMed: 11121407]
31. Zhang H, Zha X, Tan Y, et al. Phosphoprotein analysis using antibodies broadly reactive against phosphorylated motifs. J Biol Chem 2002;277:39379–87. [PubMed: 12151408]
32. Mellick AS, Day CJ, Weinstein SR, Griffiths LR, Morrison NA. Differential gene expression in breast cancer cell lines and stroma-tumor differences in microdissected breast cancer biopsies revealed by display array analysis. Int J Cancer 2002;100:172–80. [PubMed: 12115566]
33. Peng J, Wallar BJ, Flanders A, Swiatek PJ, Alberts AS. Disruption of the Diaphanous-related formin Drf1 gene encoding mDia1 reveals a role for Drf3 as an effector for Cdc42. Curr Biol 2003;13:534–45. [PubMed: 12676083]
34. Dong JT, Boyd JC, Frierson HF Jr. Loss of heterozygosity at 13q14 and 13q21 in high grade, high stage prostate cancer. Prostate 2001;49:166–71. [PubMed: 11746261]
35. Eisenmann KM, Harris ES, Kitchen SM, Holman HA, Higgs HN, Alberts AS. Dia-interacting protein modulates formin-mediated actin assembly at the cell cortex. Curr Biol 2007;17:579–91. [PubMed: 17398099]
36. Cocucci E, Racchetti G, Meldolesi J. Shedding microvesicles: artefacts no more. Trends Cell Biol 2009;19:43–51. [PubMed: 19144520]
37. Jansen FH, Krijgsveld J, van Rijswijk A, et al. Exosomal secretion of cytoplasmic prostate cancer xenograft-derived proteins. Mol Cell Proteomics. 2009
38. Tahir SA, Yang G, Goltsov AA, et al. Tumor cell-secreted caveolin-1 has proangiogenic activities in prostate cancer. Cancer Res 2008;68:731–9. [PubMed: 18245473]
39. Mukhopadhyay NK, Kim J, Cinar B, et al. Heterogeneous nuclear ribonucleoprotein K is a novel regulator of androgen receptor translation. Cancer Res 2009;69:2210–8. [PubMed: 19258514]
40. Schonichen A, Alexander M, Gasteier JE, Cuesta FE, Fackler OT, Geyer M. Biochemical characterization of the diaphanous autoregulatory interaction in the formin homology protein FHOD1. J Biol Chem 2006;281:5084–93. [PubMed: 16361249]
41. Rundle DR, Gorbsky G, Tsiokas L. PKD2 interacts and co-localizes with mDia1 to mitotic spindles of dividing cells: role of mDia1 IN PKD2 localization to mitotic spindles. J Biol Chem 2004;279:29728–39. [PubMed: 15123714]
42. Hannemann S, Madrid R, Stastna J, et al. The diaphanous related formin FHOD1 associates with ROCK1 and promotes Src-dependent plasma membrane blebbing. J Biol Chem. 2008
43. Kovar DR, Harris ES, Mahaffy R, Higgs HN, Pollard TD. Control of the assembly of ATP- and ADP-actin by formins and profilin. Cell 2006;124:423–35. [PubMed: 16439214]
44. Jurdic P, Saltel F, Chabadel A, Destaing O. Podosome and sealing zone: specificity of the osteoclast model. Eur J Cell Biol 2006;85:195–202. [PubMed: 16546562]
45. Yoshida K, Soldati T. Dissection of amoeboid movement into two mechanically distinct modes. J Cell Sci 2006;119:3833–44. [PubMed: 16926192]

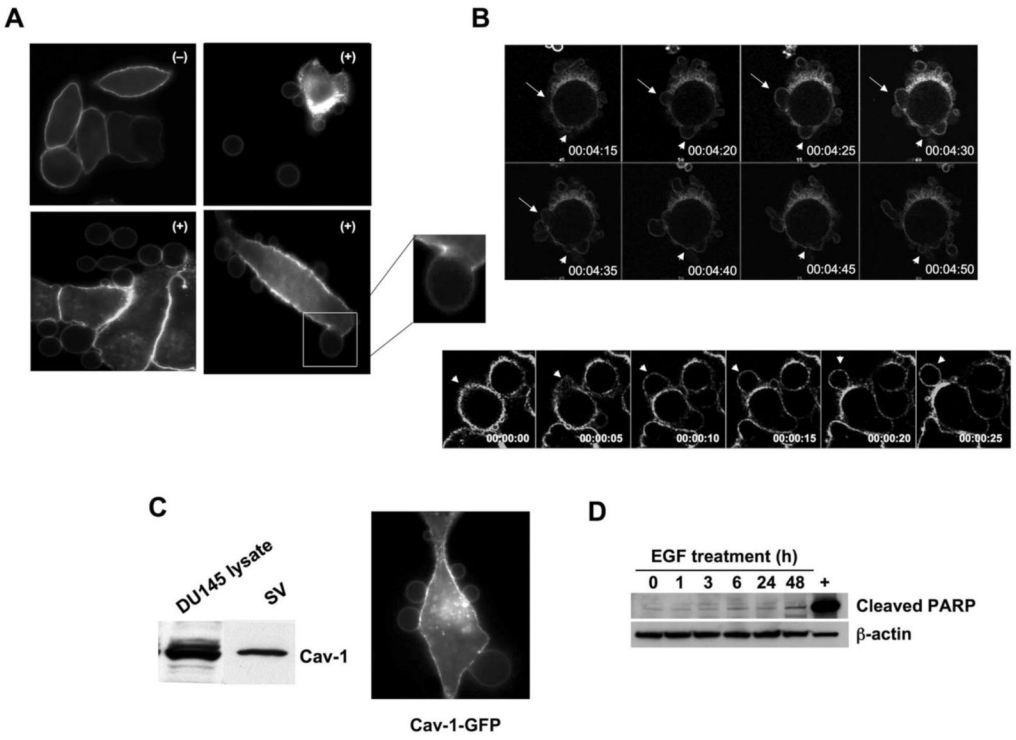

Figure 1. EGF induces formation of non-apoptotic membrane blebs

(A) Membrane staining with 0.5 μg/ml FITC-CTxB for 5 min, after 3 h treatment with: (−) vehicle or (+) EGF (50 ng/ml), and imaged by confocal microscopy (63X). All panels show DU145 cells, except the panel at upper right, which shows a PC-3 cell and vesicles shed (SV) into the medium. The inset shows a single, attached bleb at higher power. **(B)** Frames (5 sec interval) from Movies 1 and 2 acquired by real time confocal microscopy of DU145 cells expressing membrane-targeted pMEM-YFP, and treated with EGF. Panel B shows two examples (differently shaped arrows) of bleb dynamics. **(C)** Lysates from whole cells and SV contain endogenous Cav-1, consistent with localization of a Cav-1-GFP fusion to membrane blebs. **(D)** EGF does not induce apoptosis under these experimental conditions, as shown by an assay for cleaved PARP.

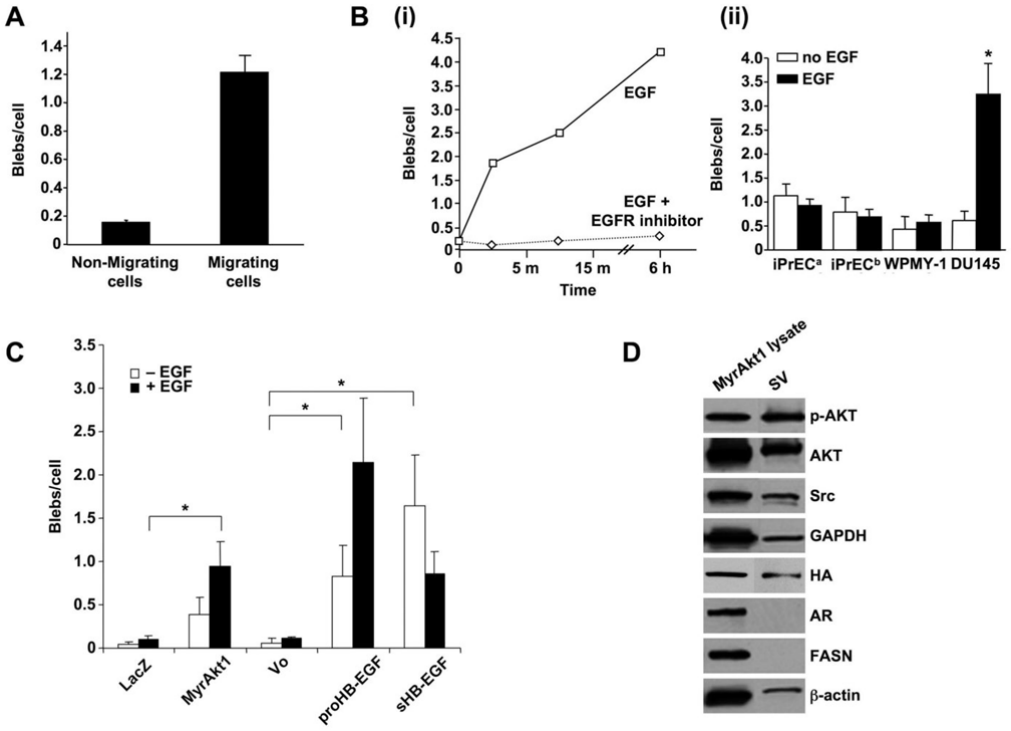

Figure 2. Blebbing is associated with cell migration, activation of signaling and results in production of shed vesicles that contain membrane proteins

(A) Bleb formation in DU145 cells treated with EGF (50 ng/ml, 12 h) in a wound healing assay. **(B) (i)** Bleb formation in DU145 cells treated with EGF or EGF plus gefitinib (ZD1839) (10 μM). **(ii)** Bleb formation in prostate normal epithelial (iPrEC) and stromal (WPMY-1) cells, in comparison with DU145, with and without EGF. iPrEC^a were kept in PrEGM medium, which is serum-free but contains EGF, while iPrEC^b were transferred to serum-free RPMI 12 h before treatment. **(C)** Bleb formation in LNCaP cells stably engineered to express MyrAkt1, pro-HB-EGF, or soluble (constitutively secreted) sHB-EGF. LacZ (irrelevant gene) and Vo (vector only) are negative controls. **(D)** Protein from whole cell lysates and SV from EGF-treated LNCaP/MyrAkt1 cells were blotted with the indicated Abs.

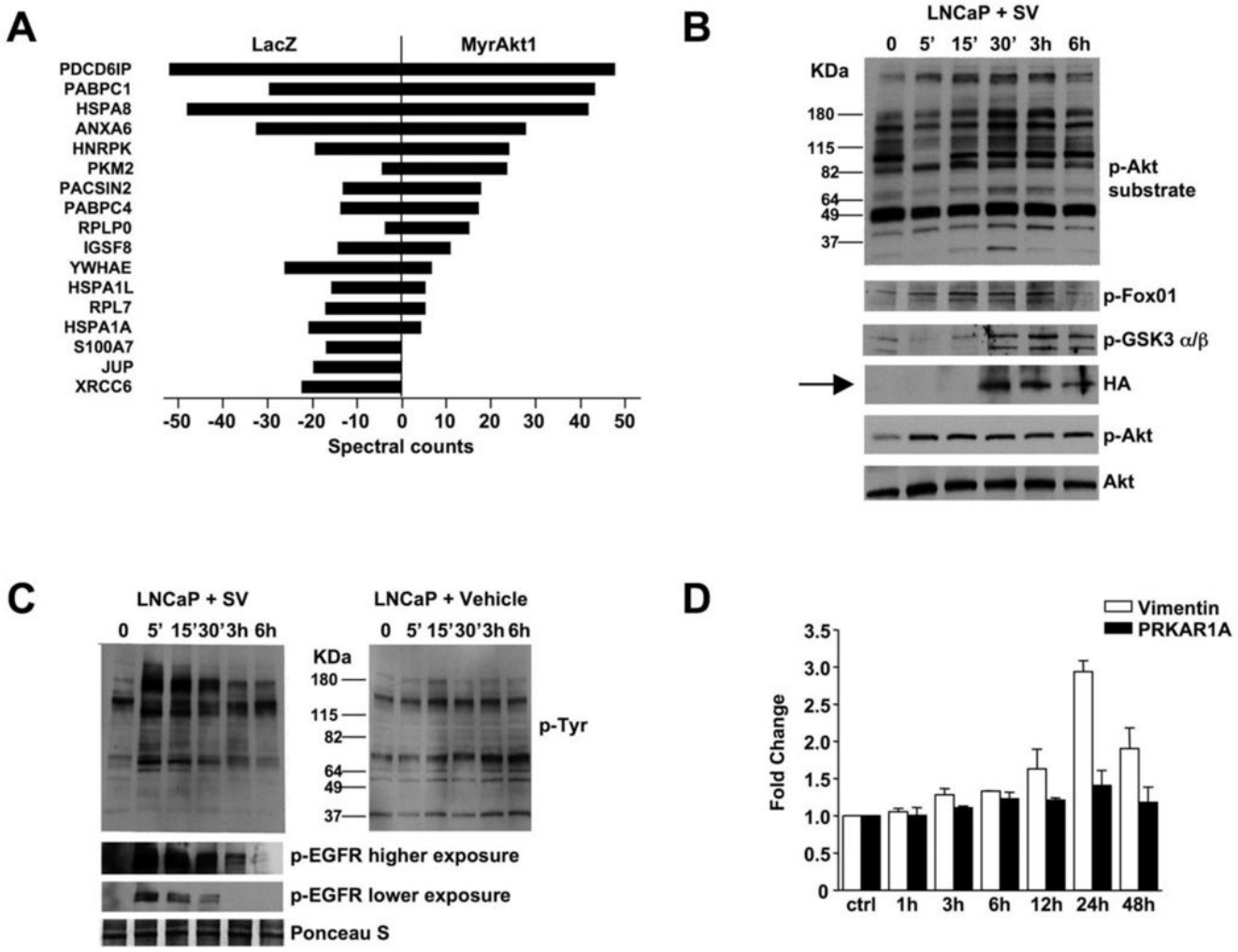

Figure 3. Shed vesicles exhibit oncosome activity

(A) Proteins identified by tandem mass spectrometry in bleb material and quantified using spectral counting. PDCD6IP (Programmed Cell Death 6 Interacting Protein), PABPC1 (Poly (A) Binding Protein, Cytoplasmic 1), HSPA8 (Heat Shock 70kDa Protein 8), ANXA6 (Annexin A 6), hnRNP-K (Heterogeneous Nuclear Ribonucleoprotein K, PKM2 (Pyruvate Kinase M2), PACSIN2 (Protein Kinase C and Casein Kinase Substrate in Neurons 2), PABPC4 (Poly(A) Binding Protein, Cytoplasmic 4), RPLPO (Ribosomal Protein Large P0-like Protein), IGSF8 (Immunoglobulin Superfamily, member 8), YWHAE (Tyrosine 3-monooxygenase/ tryptophan 5-monooxygenase Activation Protein, Epsilon Polypeptide), HSPA1L (Heat Shock 70kDa Protein 1-Like), RPL7 (Ribosomal Protein L7), HSPA1A (Heat Shock 70kDa protein 1A), S100A7 (S100 calcium binding protein A7), JUP (Junction Plakoglobin), XRCC6 (X-ray Repair Complementing defective repair in Chinese hamster cells 6). **(B)** LNCaP/LacZ cells were exposed to SV obtained from EGF-treated LNCaP/MyrAkt1 cells. Blotting of whole cell lysates is shown. **(C)** LNCaP/LacZ exposed to 20 μg of SV or vehicle from EGF-treated LNCaP/MyrAkt1 cells and assessed for p-Tyr (upper panels). The lower panels show the results of blotting with p-EGFR antibody (p-Tyr^{1068}). **(D)** WPMY-1 cells were exposed to LNCaP/ MyrAkt1 derived SV for the indicated times. Vimentin mRNA was quantified by qRT-PCR in recipient cells, and normalized using GAPDH. An irrelevant gene, PRKAR1A, was used as control.

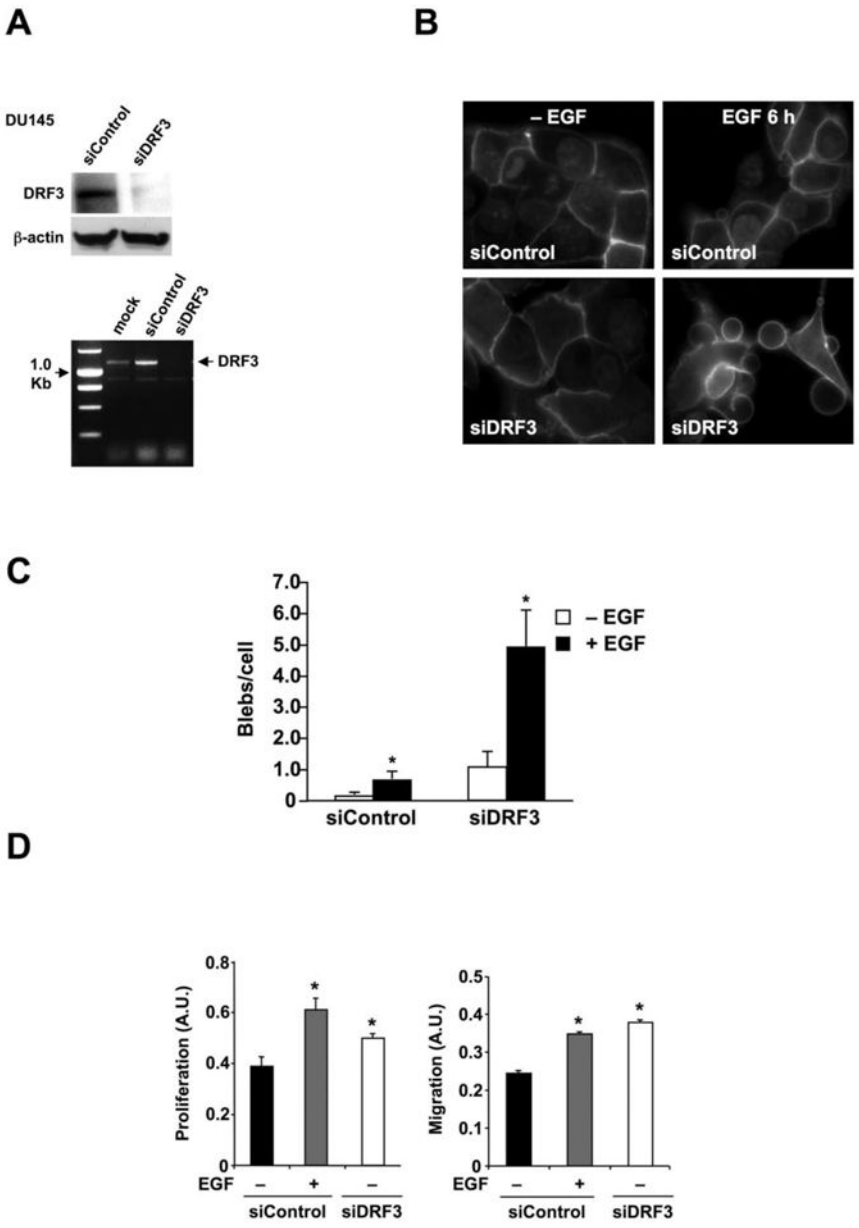

Figure 4. DRF3 knockdown by RNA interference results in oncosome secretion

(A) Verification of DIAPH3 gene silencing by siDRF3 in DU145 cells by western blot (upper panel) and RT-PCR (lower panel). Control non-targeting siRNA was a negative control. **(B)** FITC-CTxB staining of DU145 cells showing blebbing in siDRF3-transfected or siRNA control cells, with or without EGF (3 h) (right panel). **(C)** Quantitative analysis of bleb formation in DU145 cells treated with siRNA for DRF3 or control siRNA, +/− EGF. **(D)** Proliferation assay (left panel) and migration assay (right panel) in DU145 cells treated with SV prepared from DU145 cells treated with siRNA control oligos, +/− EGF, or with DRF3-targeted oligos. *$p<0.05$.

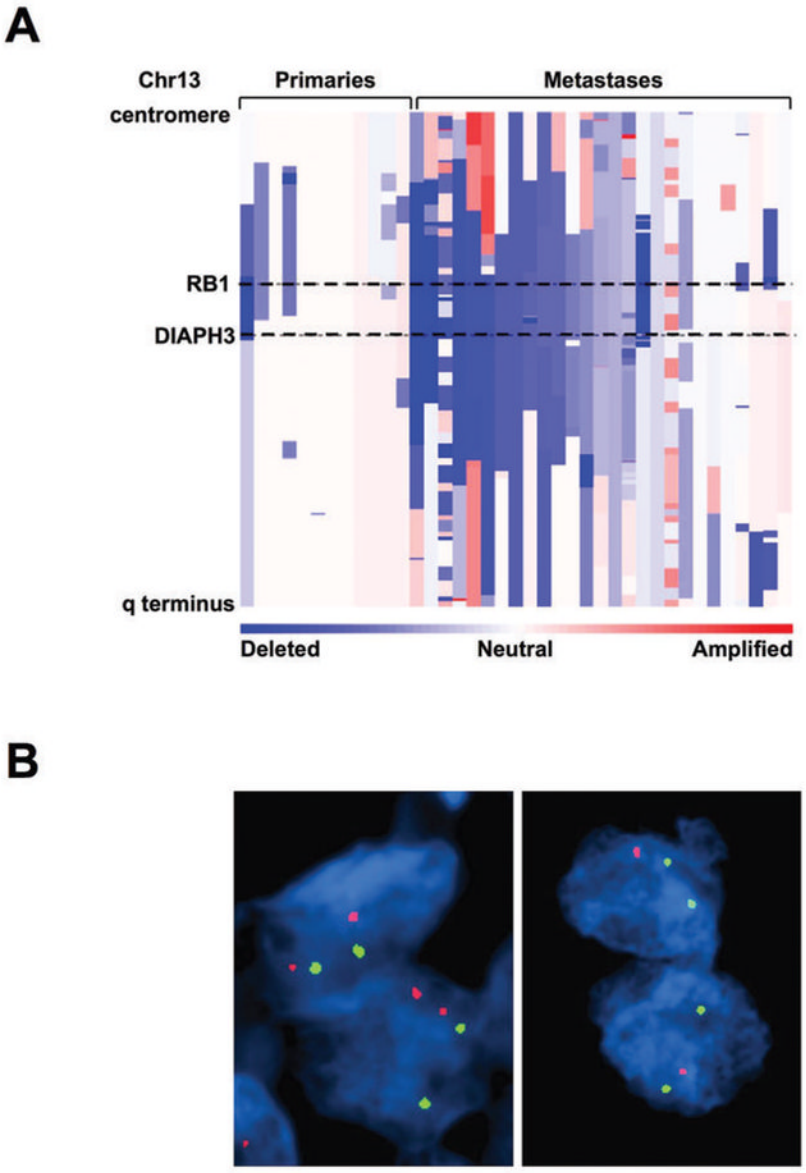

Figure 5. Genomic profiling of primary and metastatic prostate cancer at the DIAPH3 locus

(A) Amplifications (red) and deletions (blue), determined by segmentation analysis of normalized signal intensities from 100K SNP arrays (see Methods), are displayed for 39 prostate cancers (x-axis; primaries and metastases are designated along the top) for the q arm of chromosome 13 (chromosomal positions indicated along the y-axis include the centromere, q-terminus, and RB1 loci). **(B)** DIAPH3 fluorescent in situ hybridization was performed by dual color FISH on PCa tissues. The FISH image on the left shows both red signals (DIAPH3 locus on chr13q21.2) and green signals (a stable region on chr21q22.12) in representative nuclei indicating no deletion of DIAPH3 in tumor cells. The FISH image on the right shows one red signal (DIAPH3 locus on chr13q21.2) and two green signals (a stable region on chr21q22.12) in representative nuclei. Loss of the second red signal is consistent with deletion at DIAPH3. Original magnification of FISH images, 60 X objective.

Table 1

Proteins identified by mass spectrometry were analyzed by MetaCore software (GeneGo Inc.) using two algorithms in which the output is either an intracellular signaling pathway or a biological process. Significance was defined as $p<0.05$.

Pathway models	**LacZ (−log P)**	**MyrAktl (−logP)**
Translation: Elongation: Termination	3.9	(n/s)
Cytoskeleton: Regulation of cytoskeleton rearrangement	(n/s)	4.7
Cell cycle: Meiosis	(n/s)	5.9
Cytoskeleton: Cytoplasm microtubules	(n/s)	(n/s)
Inflammation: IL-6 signaling	(n/s)	4.1
DMA damage: Check point	(n/s)	4.1
Inflammation: TREMI signaling	(n/s)	3.9
Cell cycle: GI-S	(n/s)	3.6
Cell adhesion: Cell junctions	(n/s)	3.6
Transduction: Translation initiation	4.5	(n/s)
Biological process models	LacZ (−log P)	MyrAktl (−logP)
Glycolysis and gluconeogenesis	(n/s)	(n/s)
Vitamin K metabolism	(n/s)	(n/s)
Transcription: Role of heterochromatin protein(HPI) family in transcriptional silencing	(n/s)	1.5
Cell cycle: Role of 14-3-3 proteins in cell cycle regulation	(n/s)	5.7
Translation: Regulation of translation initiation	1.6	(n/s)
Cytoskeleton remodeling: Neurofilament	(n/s)	(n/s)
Glycolysis and gluconeogenesis	(n/s)	(n/s)
Transcription: Role of AP in regulation of cellular metabolism	(n/s)	(n/s)
Cell cycle: Spindle assembly and chromosome separation	(n/s)	(n/s)
Development: Role of CDKS in neuronal development	(n/s)	(n/s)

n/s: not significant